# The effect of electric double layers, zeta potential and pH on apparent viscosity of non-Brownian suspensions

Srinivasan, Sudharsan; Van den Akker, Harry E.A.; Shardt, Orest

**Important note**
To cite this publication, please use the final published version (if applicable).
Please check the document version above.

# The effect of electric double layers, zeta potential and pH on apparent viscosity of non-Brownian suspensions

Sudharsan Srinivasan[1,2] | Harry E. A. Van den Akker[1,2,3] | Orest Shardt[1,2]

[1]Synthesis and Solid State Pharmaceutical Centre (SSPC), University of Limerick, Limerick, Ireland

[2]Bernal Institute and School of Engineering, University of Limerick, Limerick, Ireland

[3]Transport Phenomena Lab, Department of Chemical Engineering, Delft University of Technology, Delft, The Netherlands

**Correspondence**
Harry E. A. Van den Akker, Synthesis and Solid State Pharmaceutical Centre (SSPC), University of Limerick, V94 T9PX Limerick, Ireland.
Email: harry.vandenakker@ul.ie

## Abstract

We carried out 3D simulations of monodisperse particle suspensions subjected to a constant shear rate with the view to investigate the effect of electrical double layers around the particles on apparent suspension viscosities. To this end, expressions for Debye length, zeta potential, and ionic strength (pH) of the liquid were incorporated into our in-house lattice Boltzmann code that uses the immersed boundary method and includes subgrid lubrication models. We varied the solids concentration and particle radius, keeping the particle Reynolds number equal to 0.1. We report on results with respect to the effect of pH in the range 9 through 12 and of Debye length on apparent viscosity and spatial suspension structures, particularly at higher solids volume fractions, and on the effect of flow reversals.

**KEYWORDS**
complex fluids, particulate flows, rheology, solids processing, suspensions

## 1 | INTRODUCTION

The flow behavior of ionic suspensions, that is, suspensions consisting of particles with electrically charged surfaces, is strongly dependent on Coulomb forces between the charged particles. Examples of such (often colloidal) ionic suspensions are various types of clays, Portland cement, latex paint, wastewater sludge, drilling mud, and distinct types of mud resulting from ore refining operations. Along with the pH of the carrier liquid,[1–3] the Coulomb forces between the (colloidal, i.e., Brownian) particles may have a drastic impact on suspension rheology as expressed in terms of a (relative) apparent viscosity and on the flow dynamics of such suspensions.

In our earlier papers,[4,5] we already reported on the use of the lattice Boltzmann (LB) technique for simulating nonionic non-Brownian particle suspensions, which is a topic reviewed earlier in detail by Aidun and Clausen.[6] In our papers, we convincingly relate apparent suspension viscosity to the dynamic behavior of revolving clusters and structures in suspensions subject to shear, for monodisperse neutrally buoyant spherical particles (order 10–100 μm) and solids fractions up to 52%. Different from experimental viscosity measurements, such detailed LB simulations allow for an inner view on the details of the response of the particles to the imposed shear, as also reported earlier.[6] The dynamics of the revolving clusters we found at finite particle Reynolds numbers of order $10^{-1}$ is due to advection, rotation, and collisions of both individual particles and clusters. The average relative apparent viscosities found in our LB simulations closely followed the correlation due to Krieger and Dougherty[7] and the data reported by Sierou and Brady[8] and Thorimbert et al.[9]

In ionic suspensions, the phenomena are different, however. In the classical Derjaguin–Landau–Verwey–Overbeek (DLVO) theory,[10–13] the surface charge of a particle attracts counter-ions in the liquid to form a diffuse electric double layer (EDL) around each particle. The net charge within an EDL is opposite to that of the particle surface; it decays with increasing distance from the particle
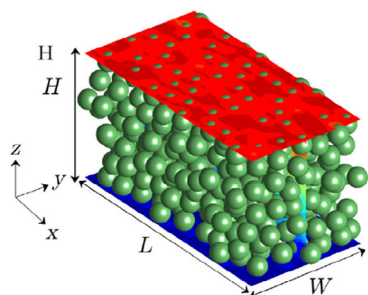
surface. The thickness of this EDL is expressed in terms of the so-called Debye length denoting the distance over which the potential decreases by a factor $e$. In our cases of interest, the Debye length is of the order of 0.01 μm. When the EDLs of two (or more) like-charged particles are at the verge of overlapping, a repulsive force results which may keep the particles separated. All this implies that the ion strength (pH) of the carrier liquid also plays a role.

To the best of our knowledge, the literature on computational modeling of the effect of ionic forces on the flow behavior of finite-inertia moderately dense suspensions is very limited, and no relevant experimental data seem to be available for validation purposes. Most researchers developing numerical approaches of the flow characteristics of (charged) particle suspensions ignore the role of ionic forces due to surface potentials and EDLs, and just consider hydrodynamic and frictional models. Earlier,[14] We explained how we incorporated the extra DLVO forces into our[4,5] immersed boundary (IB) LB code.

When simulating non-Brownian particles of order 10–100 μm on an LB lattice, the EDL's thickness of just some 0.01 μm means that the DLVO forces cannot be resolved when using a practical number of lattice nodes. As a result, incorporating the DLVO forces requires subgrid scale models alongside the much more common hydrodynamic lubrication subgrid scale models. We found[14] that the close-range attractive Van der Waals forces can safely be ignored due to the dominating role of the repulsive forces which keep the non-Brownian particles sufficiently separated.

While in our 2022 paper,[14] we analyzed computational results with respect to the impact of Debye length on viscosity and structures at various solids volume fractions at pH = 11 (ionic strength $10^{-3}$ mol/L); in this paper, we report on results with respect to the effect of pH and EDLs on relative apparent viscosity and spatial suspension structures, particularly at higher solids volume fractions, and on the effect of flow reversals which are thought of as being indicative of the response of an ionic suspension to dynamic processing conditions.

To this end, we used the same computational set-up of a quasi-Couette viscometer flow domain (see Figure 1) as before, with the (red) upper wall moving to the right (in the positive $x$-direction), the (blue) bottom wall to the left, and with periodic walls in the $x$- and $y$-directions. This implies that we calculate the apparent viscosity of the suspension from the shear stress between the suspension and the two moving walls, just like in a real viscometer. By taking this approach we do not pursue the technique of the Lees–Edwards boundary condition for a triply periodic linear shear field, which is more accurate for finding the bulk rheological properties in the absence of walls.[6,15] An advantage of our approach is that there is no need to calculate the stresslets exerted the fluid flow on all particle surfaces of the suspension.[16]

Prior to reporting about our findings, we now first present the main features of our LB flow solver including the IB model for tracking all particle motions, the DLVO equations for dealing with pH and EDLs, and all parameter values used as input in our simulations.

## 2 | SIMULATION METHOD AND INPUT

### 2.1 | Our LB fluid flow solver

Since we described the models used in the simulations of current interest in quite some detail in our earlier papers, we report here just some of their main features; for details, we refer to our earlier papers. The incompressible Navier–Stokes equations for the flow field of the carrier liquid is solved by using the LB method[17] with the Bhatnagar–Gross–Krook (BGK) collision operator on a $D3Q19$ lattice. The Ladd[18,19] bounce-back scheme with momentum correction enforces the no-slip condition at the sliding walls on top and bottom of the quasi-Couette viscometer flow domain.

The no-slip condition at the surface of all particles is enforced by adopting the IB method of Feng and Michaelides[20] in which the surface of a particle is represented by sets of equally spaced Lagrangian marker and reference points. In each simulation step, the marker points are advected by the fluid, and any displacement between a marker point and its corresponding reference point leads to a Lagrangian force. This method, described and tested in detail before,[4] exploits a linear interpolation scheme[21] and the Shan and Chen forcing scheme[22] in order to match the local fluid velocity with the translational and rotational particle velocities. Embedding the motion and rotation of these spherical particles onto a regular LB lattice results in a hydrodynamic radius some 5% larger than the input radius. Therefore, for calculations of the distances between surfaces (both particle–particle and particle–wall), we use the hydrodynamic radius, in agreement with Aidun and Clausen.[6]

Since particles may approach each other due to their individual advection and rotation rates, we have to model the interstitial fluid motions and the mutual fluid-particle forces acting on distances smaller than the lattice spacing used in the simulation. So-called sublattice scale lubrication model corrections to forces and torques (denoted by NTLC which stands for Normal and Tangential Lubrication Corrections) are needed to capture the missing effects of the



**FIGURE 1** The flow domain used in our simulations, mimicking in terms of domain geometry, flow conditions, and number of particles in a Couette type of viscometer. The red upper wall moves in the positive $x$-direction (to the right), while the lower blue wall moves to the left. In the other two directions, periodic walls are used.

unresolved flow field. The reader is referred to our earlier papers for the model equations. Of course, in our IB–LB code, we only add the differences between under-resolved LB values and analytical terms, these differences being denoted as lubrication corrections (LCs).

We apply the so-called lubrication cutoff distances $h_O$ to decide when to turn on (or switch off) these LCs. The normal, tangential translational, and rotational lubrication cutoffs are $h_o^n/R_{hyd} = 0.5$, $h_o^t/R_{hyd} = 0.1$, and $h_o^r/R_{hyd} = 0.01$, respectively. The reader is referred to our earlier papers and to Srinivasan's PhD thesis[23] for the expressions and the details of the procedure. For particle–wall interactions, LCs are applied for gaps $h^{tw}$ and $h^{rw}$ between particle and wall smaller than $0.1R_{hyd}$ rather than $0.01R_{hyd}$ as in Srinivasan et al.[14]

We integrated the linear and angular motions of the particles to find their positions by means of an explicit leapfrog scheme. To ensure the stability of the integration scheme, we used constant subtime stepping for dilute-to-moderate suspensions and an adaptive scheme for dense suspensions. For the sake of simulation speed, we applied a binning algorithm to calculate the subgrid scale forces only for particles within a specified mutual distance.[24,25]

The relative apparent viscosity is computed from the resolved and unresolved wall (top and bottom) shear stress at either moving wall:

$$\eta_r = \frac{\langle T_w^{LB} \rangle + T_w^{lub}}{\mu \gamma},$$

where the first term in the numerator denotes the wall shear stress averaged over a single wall as computed from the LB simulation and the second term stands for the shear stresses due to the LC forces between particles and this wall. Then we average twice: first because of the two walls and second due to the fluctuations over time. The result is denoted by $\overline{\overline{\eta}}_r$.

## 2.2 | The DLVO forces

Given the very low values of the ratio of EDL thickness to hydrodynamic radius $R_{hyd}$, also the repulsive DLVO forces are sublattice.

The Debye length—that is, the thickness of an EDL—is denoted by $\kappa^{-1}$ and depends on the dielectric permittivity $\varepsilon$ of the liquid, the Boltzmann constant $k_B$, the absolute temperature $T$, the valence $Z$ of the ions (we only use $Z = 1$), the fundamental charge $e$ (being $1.6\cdots10^{-19}$ C) and the number density $\eta_\infty$ of the ions, according to

$$\kappa^{-1} = \sqrt{\frac{\varepsilon k_B T}{2(Ze)^2 \eta_\infty}}. \tag{1}$$

For water at room temperature, this expression can be reworked[12] into

$$\kappa^{-1} = \frac{0.304}{Z\sqrt{I}} \quad \text{(in nm)}, \tag{2}$$

in which $I$ denotes the ionic strength of the liquid in mole/L. The larger the ionic strength (higher pH for basic solutions), the more the ions screen the charged particle surface and the thinner the Debye length.

In the DLVO model, the repulsive force between two spheres $p$ and $q$ is given by

$$F_p^r = -\frac{64\pi\eta_\infty k_B T \gamma_\delta^2 R_{hyd}}{\kappa} \exp(-\kappa h) \, \widehat{n}_{pq}, \tag{3}$$

in which $h$ stands for the gap between the two particles,

$$n_{pq} = \frac{X_q - X_p}{\|X_q - X_p\|} \tag{4}$$

denotes the unit vector pointing from the center of $p$ to the center of $q$, and

$$\gamma_\delta^2 = \tanh\left(\frac{Ze\psi_\delta}{4k_B T}\right) \tag{5}$$

with $\psi_\delta$ denoting the zeta potential, the value of which may depend on the pH of the liquid as well.

Similarly, the repulsive DLVO force $F_p^r$ between a particle and a wall of the domain is given by

$$F_p^r = -\frac{128\pi\eta_\infty k_B T \gamma_\delta^2 R_{hyd}}{\kappa} \exp(-\kappa h) \, \widehat{n}_{pw}. \tag{6}$$

These forces are switched on at $h < 0.1R_{hyd}$.

## 2.3 | Input parameters

We performed simulations for suspensions up to 52% solids fraction subjected to constant simple shear conditions in a box, periodic in the x- and y-directions, H being the spacing (in the z-direction) of the two walls moving in opposite directions (see Figure 1). The size of the LB lattice was $L \times W \times H = 208 \times 104 \times 104$ (in lu). Two particle sizes were studied, viz. 10 and 150 μm in radius, starting from a regular cubic distribution with random perturbation, with confinement ratio $\delta = 2R/H$ being equal to 0.15. For both particle sizes, we used 8 lu for the particle radius which results in $R_{hyd} = 8.65$ lu. In all simulations, the particle Reynolds number, $Re_p$, was kept at the value 0.1.

Table 1 shows the parameter values used in all simulations.

As we ran our simulations for pH = 9, 10, 11, and 12, Table 2 presents the values, both in physical units and in rescaled LB units, for Debye length $\kappa^{-1}$, number density $\eta_\infty$ and thermal energy $k_B T$, depending on pH. According to Liu et al.,[26] the zeta potential of iron oxide particles suspended in sodium hydroxide solution varies between $-30$ and 30 mV, for which $\gamma_\delta^2 = 0.1$. We will compare our results for $\psi_\delta = +30$ mV, with results obtained for uncharged

**TABLE 1** Variables and values of several simulation parameters.

| Variable | Description | Physical units | LB units |
|---|---|---|---|
| $\nu$ | Kinematic viscosity | $10^{-6}$ m$^2$/s | $1/30$ lu$^2$/ts |
| $\rho$ | Density | 1000 kg/m$^3$ | 1 mu/lu$^3$ |
| lu | Lattice spacing | $1.25 \times 10^{-6}$ m | 1 lu |
| | | $1.875 \times 10^{-6}$ m | |
| $R$ | Particle radius | $10 \times 10^{-6}$ m | 8 lu |
| | | $150 \times 10^{-6}$ m | |
| ts | Lattice time | $5.2 \times 10^{-8}$ s | 1 ts |
| | | $1.17 \times 10^{-5}$ s | |
| $\dot{\gamma}$ | Shear rate | $807$/s | $4.2 \times 10^{-5}$/ts |
| | | $3.6$/s | |

*Note*: The units of length, time, and mass are expressed as lu, ts, and mu, respectively. Variables that depend on the particle size are divided into two rows where the value of the top row corresponds to 10-μm particles and the bottom row corresponds to particle size 150 μm.

suspensions ($\psi_\delta = 0$ and $\gamma_\delta^2 = 0$) and for a very high zeta potential, viz. $\psi_\delta = 175$ mV and $\gamma_\delta^2 = 0.9$.

## 3 | RESULTS

### 3.1 | Time evolution of apparent viscosity

After the two walls have been set into motion, in opposite directions, the arbitrary cubic arrangement of solid particles (initially at rest) for a given solids volume fraction starts adapting to the new situation. Soon after the start of the shear, the relative apparent viscosity $\overline{\eta}_r$ attains a value of about 5. Then, obviously, some rearrangement of the particle structure takes place which may depend on pH and on the EDLs around the particles, that is, on the LB parameter $\kappa R_{hyd}$ which represents the combined effect of pH, EDL, and particle size.

Figure 2 then presents plots of the time evolution of $\overline{\eta}_r$ for four different values of $\kappa R_{hyd}$, all at $\psi_\delta = 30$ mV, for 52% solids volume fraction. The upper two panels in Figure 2 relate to pH = 10, the lower two panels to pH = 12. In each panel, also the time evolution for the extreme value $\psi_\delta = 175$ mV is included.

All simulations were run for a sufficiently long duration, such that eventually steady fluctuations about a more or less constant value for $\overline{\eta}_r$ were attained. These steady viscosity values coincide with those at $\psi_\delta = 175$ mV, except for $\kappa R_{hyd} = 355$, where the difference in the eventual viscosity values amounts to some 30%. In the simulation for $\kappa R_{hyd} = 355$, also the evolution of $\overline{\eta}_r$ for $\psi_\delta = 30$ mV is very different from that for $\psi_\delta = 175$ mV. An explanation for this deviating behavior could be in the use of an adaptive time-stepping method for $\psi_\delta = 30$ mV and $\kappa R_{hyd} = 355$, as in this simulation the integration of particle motion using a constant time-stepping algorithm was unstable. It looks as if with adaptive time stepping the eventual constant value of $\overline{\eta}_r$ is attained faster and along another path. In all other cases, we used constant time-stepping.

**TABLE 2** Variables and values of simulation parameters for two different values of particle radii (10 and 150 μm) in both physical and LB units.

| Variable | Physical units | | pH = 9 | | pH = 10 | | pH = 11 | | pH = 12 | |
|---|---|---|---|---|---|---|---|---|---|---|
| | | | Physical | LB | Physical | LB | Physical | LB | Physical | LB |
| $k_B T$ | $3.77 \times 10^{-21}$ J | | | | | | | | | |
| | LB units | | | | | | | | | |
| | $3.4 \times 10^{-9}$ mu lu$^2$/ts$^2$ | | | | | | | | | |
| | $2.23 \times 10^{-10}$ mu lu$^2$/ts$^2$ | | | | | | | | | |
| $\kappa^{-1}$ | | | $96.1 \times 10^{-9}$ m | $\frac{1}{13}$lu | $30.4 \times 10^{-9}$ m | $\frac{1}{41}$lu | $9.61 \times 10^{-9}$ m | $\frac{1}{130}$lu | $3.04 \times 10^{-9}$ m | $\frac{1}{411}$lu |
| | | | | $\frac{1}{137}$lu | | $\frac{1}{616}$lu | | $\frac{1}{1950}$lu | | $\frac{1}{6167}$lu |
| $\kappa R_{hyd}$ | | | — | 113 | — | 355 | — | 1124 | — | 3556 |
| | | | | 1687 | | 5335 | | 16,867 | | 53,344 |
| $\eta_\infty$ | | | $6.022 \times 10^{21}$/m$^3$ | $1.1 \times 10^4$/lu$^3$ | $6.022 \times 10^{22}$/m$^3$ | $1.1 \times 10^5$/lu$^3$ | $6.022 \times 10^{23}$/m$^3$ | $1.1 \times 10^6$/lu$^3$ | $6.022 \times 10^{24}$/m$^3$ | $1.1 \times 10^7$/lu$^3$ |
| | | | | $3.9 \times 10^7$/lu$^3$ | | $3.9 \times 10^8$/lu$^3$ | | $3.9 \times 10^9$/lu$^3$ | | $3.9 \times 10^{10}$/lu$^3$ |

*Note*: The pH of the electrolyte solution is 9, 10, 11, and 12, and the ionic strengths, $I$, are $10^{-5}$, $10^{-4}$, $10^{-3}$, and $10^{-2}$ mol/L, respectively.
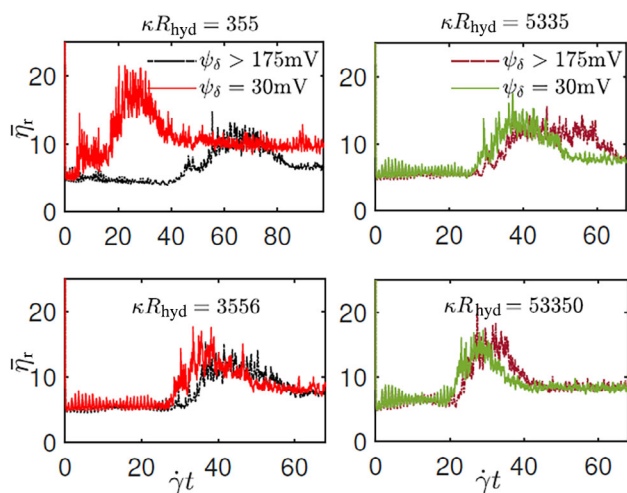
**FIGURE 2** The effect of zeta potential $\psi_\delta$ on the evolution of relative apparent viscosity for suspensions at 52% solids, at $\psi_\delta = 30$ mV (red and green), is presented for several magnitudes of $\kappa R_{\text{hyd}}$ ranging from 355 to 53,350. These results are compared to the results obtained by the simulations for an extreme value $\psi_\delta > 175$ mV (in black and purple). The upper row is at pH = 10, and the lower row is at pH = 12 (see Table 2). In all cases, $Re_p = 0.1$.

## 3.2 | Effect of pH on apparent viscosity

Figure 3 illustrates how pH, via the parameter $\kappa R_{\text{hyd}}$, affects how the eventual relative apparent viscosity $\overline{\overline{\eta_r}}$ of suspensions for two particle sizes depends on solids volume fraction. Note that for pH = 9, we only measured the apparent viscosity at 52% solids. We compare our new viscosity data with the Krieger and Dougherty correlation.[7] Up to 43% solids, the viscosities of the current work, that is, with EDLs, still largely follow the Krieger and Dougherty correlation[7] and the values reported in the literature without EDL forces. For solids fractions in excess of 43%, however, time-averaged apparent viscosities start leveling off.

Our earlier[14] relative apparent viscosities for suspensions without EDLs (i.e., with $\kappa R_{\text{hyd}} = \infty$)—and with the particle–wall lubrication cutoff always turned on when the gap is smaller than or equal to $0.01R_{\text{hyd}}$—are also included and are consistently higher than the current values with EDLs. Probably, EDLs reduce the tendency of particles to agglomerate and cluster, resulting in less effective cross-flow momentum transport.

We speculate that the reason for the leveling off behavior is in changes in morphology, that is, in the structural distribution of particles within dense suspensions. As the mean center–center distance between the particles has decreased at such high solid loading, there is little space left for free movement of the particles. In addition, the EDL forces hold the particles apart over the Debye length, excluding the options of agglomerating and clustering. The particles are trapped in a configuration of hexagonal structures (see Figure 6) which can hardly be sheared or broken by shear forces. As a result, the apparent viscosity tends to level off and remain lower than without these EDLs.

Note that in our Figures 2 and 3, the (eventual steady) values of the relative viscosities at 52% solids are in the range 7–10; while in
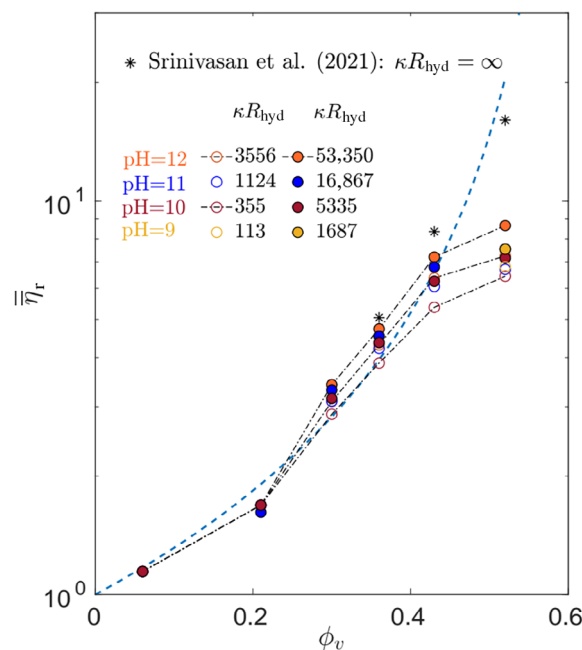


**FIGURE 3** Time-averaged relative apparent viscosity at $Re_p = 0.1$ as a function of solids volume fraction. The open circles of varying color represent suspension viscosities due to including electric double layers (EDLs) of varying thickness and strength. The dashed curve represents the Krieger and Dougherty correlation[7] with $\phi_C = 0.6$, while the asterisks denote our 2021 data obtained with normal and tangential lubrication corrections in the absence of EDLs and with the particle–wall lubrication cutoff always turned on when the gap is smaller than or equal to $0.01\ R_{\text{hyd}}$.

the simulations (at pH = 11) presented in our 2022 paper,[14] the eventual value of $\overline{\overline{\eta_r}}$ was about 5. At that time, we used a different value for the lubrication cutoff distances between particles and wall. Such differences in cutoff distances may result in slightly different configurations of clusters and therefore in different apparent suspension viscosities.

For a given particle size, increasing pH from 9 to 12 results in increasing values of ionic strength $I$ (see Table 2) and increasing values for $\kappa$ (see Equation 2), corresponding to decreasing thicknesses of the EDLs. The expression of Equation (6) for the repulsive force between particles, however, not only contains $\kappa$, both in the denominator and in the exponential expression, but also, in the numerator, the number density $\eta_\infty$ of the ions which strongly depends on pH. This results in competing effects of $\kappa$ and $\eta_\infty$ on repulsive forces and eventually on apparent viscosity. Figure 4 illustrates that at $\phi_v = 52\%$ solids the apparent viscosity exhibits a minimum at about pH = 10. Because of a lack of data at pH = 9, we cannot conclude (in Figure 3) about such a minimum for all $\phi_v > 30\%$.

## 3.3 | Effect of pH on spatial structures

In order to explain the mechanics behind the above reported observations of suspension behavior, particularly the effect of EDLs at varying pH, the 3D structure of the particle suspensions is analyzed for cases
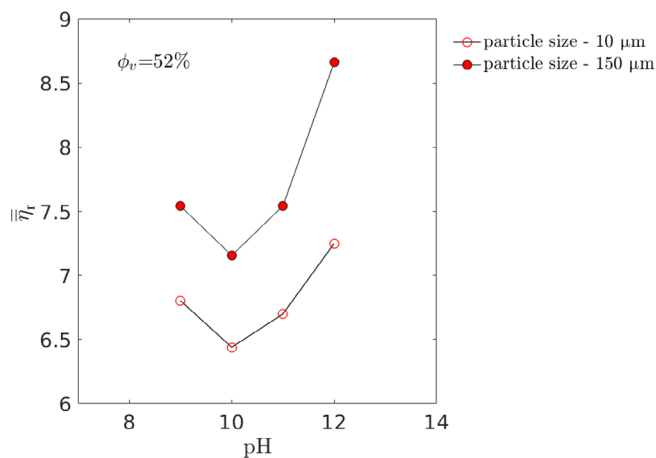
**FIGURE 4** Effect of pH on the relative apparent viscosity of the suspension at 52% solids for two particle radii, 10 and 150 μm, respectively, with $Re_p = 0.1$. It is evident that the apparent viscosity exhibits a minimum at pH = 10 for both particle sizes.

with just NTLCs activated (in the current code obtained with $\kappa R_{hyd} = \infty$) and with contributions of both NTLC and EDL forces. Since in Figures 3 and 4, the effect of EDLs and pH is most obvious for solids fractions of 43% and 52%, we will focus on these two concentrated slurries. Typical 3D particle structures are displayed in Figures 5 and 6 for two types of lateral views through the suspension, viz., through the $y - z$ and $x - z$ planes. In the upper parts of these two figures, the left column relates to pH = 11 and the right column to pH = 12, while the bottom parts repeat the structures reported by Sudharsan et al.[14] in the absence of EDLs. In order to show the distribution of particles more clearly, in all of these snapshots, the spheres are drawn at half their real size.

In the absence of EDL forces (see bottom rows of Figures 5 and 6), even though the layering of the particles is evident near the walls, the particles are mixed and form clusters in the bulk of the domain. Both types of planar views in Figure 5 demonstrate that, already at 43% solids, decreasing values of $\kappa R_{hyd}$, that is, thickening EDLs, result in particles tending to organize themselves in layers and even chains
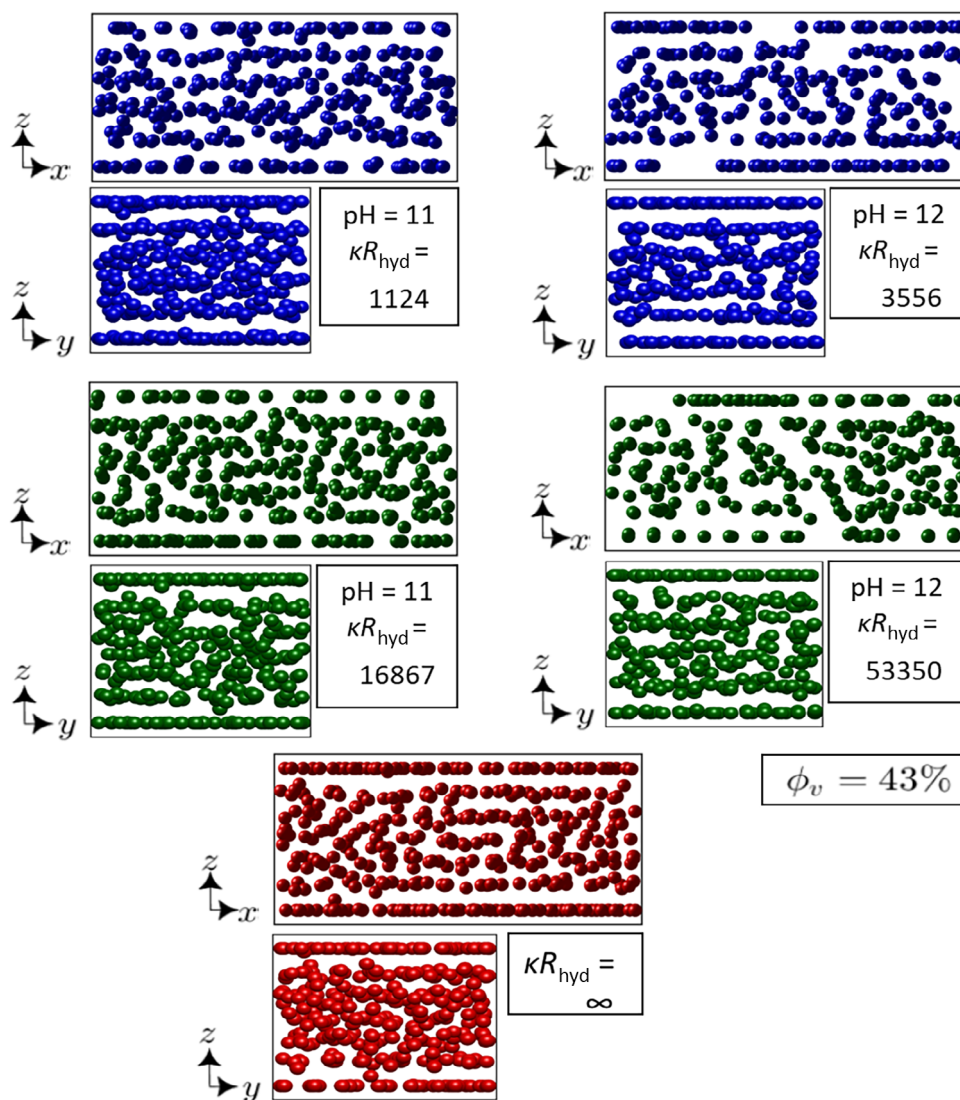


**FIGURE 5** Five panels, each showing two lateral snapshot views through the suspension at $\phi_v = 43\%$, with particles shown at half their real size; left column with two panels at pH = 11, right column with two panels at pH = 12, different values for $\kappa R_{hyd}$ as indicated; lower panel without electric double layer (EDL)[14]; maximum effect of EDL at each pH in upper row, effect of EDL higher at pH = 12.

rather than in clusters. The impact of EDLs is stronger at pH = 12 than at pH = 11. For 52% solids, Figure 6 shows this layering even more convincingly, while the $y - z$ views clearly visualize regular hexagonal arrangements of particle chains such that their mutual distances (in a normal plane) are maximum and the associated interaction energy between the chains is minimum. The formation of these hexagonal structures looks more pronounced with thicker EDLs and at pH = 12.

It would be worthwhile to quantify the effect of EDLs on the formation of these particle chains at varying pH such that the differences between the panels in Figures 5 and 6 become more explicit. We did such a quantification effort before, in our 2021 paper, in terms of average cluster size and a pair distribution function to study the effect of solids fraction on cluster formation. Now, we refrained from such an attempt as it is not quite obvious how to numerically express the change in 3D morphology. Anyhow, the visualizations of Figures 5 and 6 confirm the qualitative correctness of our speculations presented after Figure 3 with respect to the underpinning reason for the leveling off of apparent viscosity due to EDLs.

Unfortunately, we are not aware of relevant experimental data as to ionic non-Brownian particle suspensions which could validate our numerical findings. As a matter of fact, the lack of experimental guidance from literature was exactly the motivation for our current and previous work.

## 3.4 | Effects of flow reversal

Srinivasan et al.[5] also investigated the sensitivity and the response of suspension structures to disruptions in the flow field. A typical
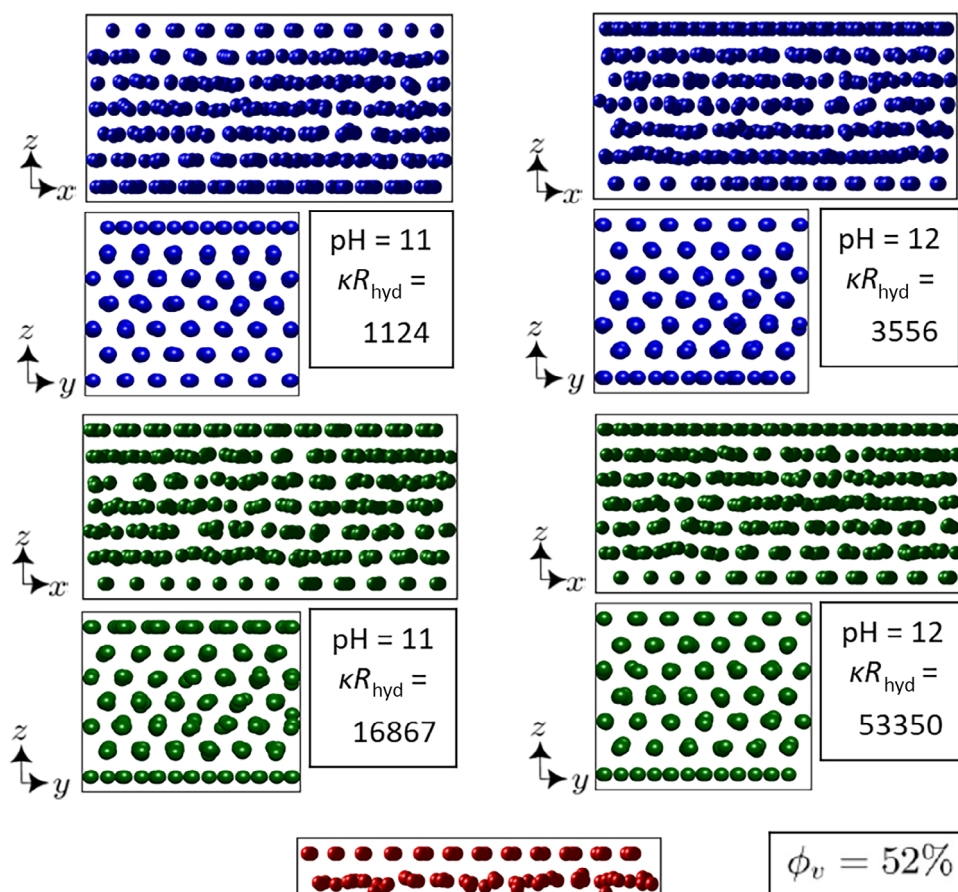


**FIGURE 6** Five panels, each showing two lateral views through the suspension at $\phi_v = 52\%$, with particles shown at half their real size; left column with two panels at pH = 11, right column with two panels at pH = 12, different values for $\kappa R_{hyd}$ as indicated; lower panel without EDL[14]; maximum effect of EDL at each pH in upper row, effect of EDL higher at pH = 12.
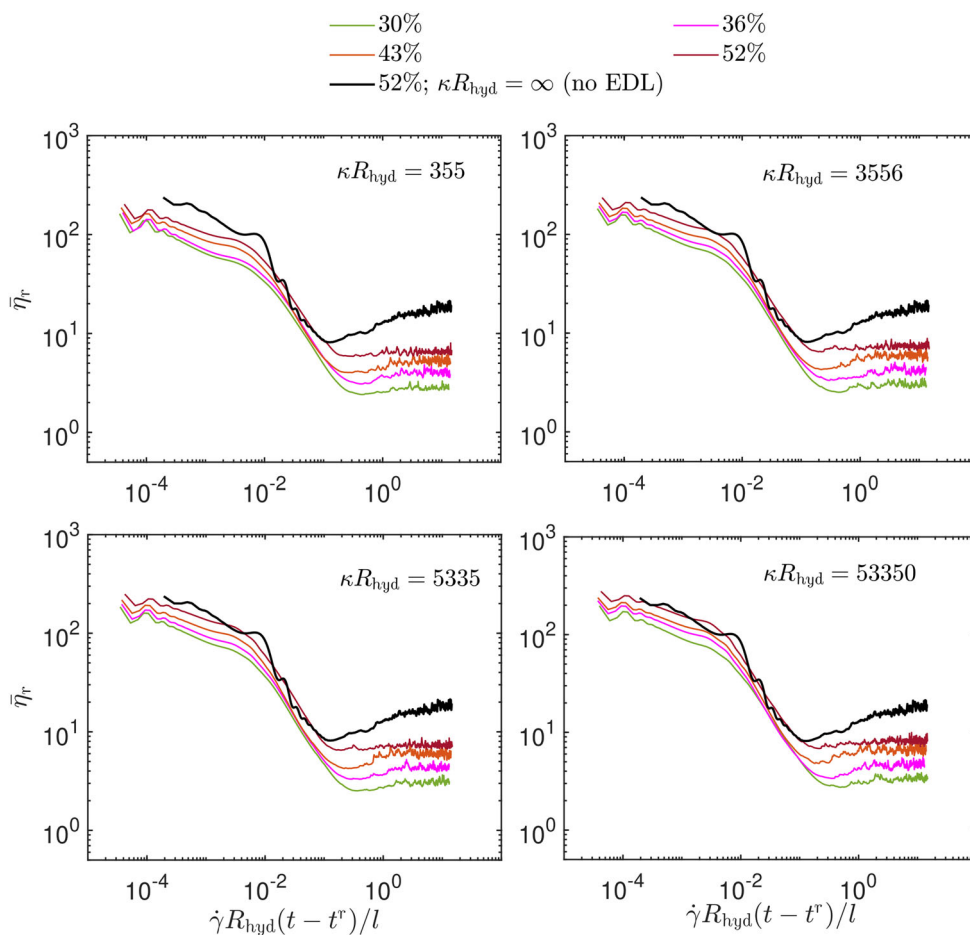
**FIGURE 7** Evolution of the average relative apparent viscosity after flow reversal versus the advective time scale[5] for solids suspensions with varying values of the nondimensional Debye length, $355 \leq \kappa R_{\text{hyd}} \leq \infty$ and for particle volume fraction, $30\% \leq \phi_v \leq 52\%$. In all cases, $Re_p = 0.1$. The length scale $l$ stands for the average particle center to particle center distance, while $t^r$ denotes the moment of flow reversal.

procedure is to apply a sudden flow reversal, as done before by many authors such as Gadala-Maria and Acrivos.[27] We now repeat our earlier analysis while including EDL forces on top of the NTLCs of our earlier study. This way, the effect of these extra repulsive forces on both the relative apparent viscosity and the stability of structures is examined, more specifically with respect to the effect of EDLs on the time period it takes for restructuring the suspension to a new equilibrium.

We started our new reversal simulations with particles at rest in a cubical arrangement with random perturbations from a perfect cubic structure. Suspensions with solids concentrations ranging from 30% to 52% were simulated for $Re_p = 0.1$. All suspensions were sheared for a sufficiently long period, say until $\dot{\gamma}t \approx 67$, to ensure steady fluctuations of the viscosity. At $\dot{\gamma}t \approx 67$, the motions of the upper and lower walls were reversed, resulting in an expected breakdown of agglomerates and structures and a high wall shear stress. Then the simulation was continued until $\dot{\gamma}t \approx 100$.

Figure 7 presents the average relative apparent viscosity (calculated from the shear stresses on the top and bottom walls) as a function of nondimensional advective time for several values of $\kappa R_{\text{hyd}}$ and of solids volume fraction. For all conditions, viscosity drops rather sharply immediately after the flow reversal. Although, after this drop, viscosities in the absence of EDLs (denoted as $\kappa R_{\text{hyd}} = \infty$ and presented by the black curves for 52% solids) go through a minimum before increasing again to a steady average

value, this minimum is more or less absent when EDLs are included in the simulation.

This suggests that EDLs prevent a complete rearrangement of the earlier chain-like structures as a result of which the effect of EDL forces is to restore a stable structure faster, while in the absence of EDLs the suspension requires approximately 2–4 advective time scales to regain a stable structure. Figure 7 also shows that the eventual stable value of the relative apparent viscosity after the flow reversal is in the range 3–7, depending on $\kappa R_{\text{hyd}}$ and solids fraction. These values are also lower than viscosities in suspensions without EDLs, exactly as found in Figure 3. Overall, we conclude the higher the solids fraction, the larger the effect of pH and EDLs.

The above explanation of the process of flow reversal in terms of reshuffling agglomerates, clusters, and structures is supported by Figure 8 in which snapshots of cross-sections through the suspension just prior to the flow reversal ($\dot{\gamma}t \approx 67$) and at the end of the simulation ($\dot{\gamma}t \approx 100$) are shown. Only the representative case of pH = 12 is considered, with $\kappa R_{\text{hyd}} = 3556$, and solids fractions of 43% and 52%.

At 43% solids, the particles are structured as homogeneous chains both before and a long time after shear reversal. When the concentration of solids is increased toward 52%, the EDL forces transform the arrangement of particles from chain-like structures into hexagonal arrangements both right before and a long time after the flow reversal. We speculate that the reason why we do not observe a minimum viscosity after flow reversal at 52% solids is in the regular

**FIGURE 8** Four panels, each showing two lateral views through the suspension at pH = 12 with $\kappa R_{\text{hyd}} = 3556$, with particles shown at half their real size; upper two panels at $\phi_v = 43\%$, lower two panels at 52%; left column before flow reversal ($\dot{\gamma} t = 67$), right column sufficient time after flow reversal ($\dot{\gamma} t = 100$).
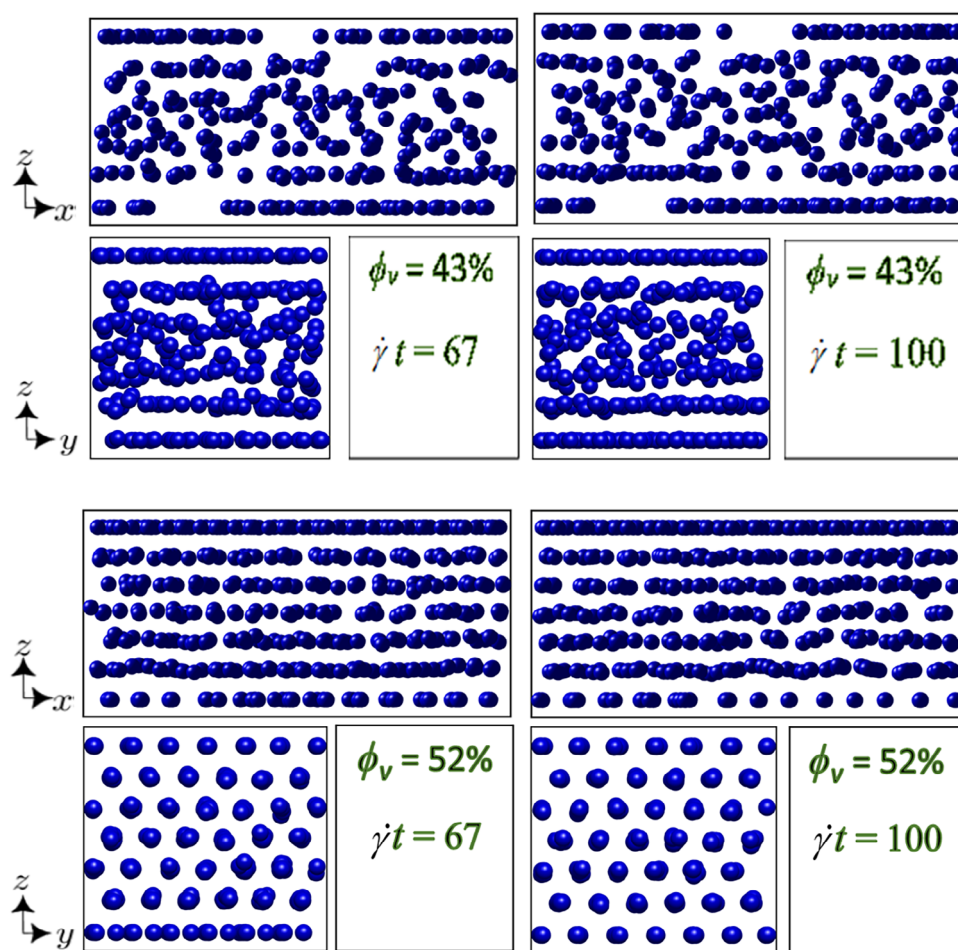


hexagonal structures. The hydrodynamic forces (both resolved and unresolved NTLC) during flow reversal may be too weak to collapse the hexagonal structure prior to reversal, to the effect that the suspension recovers its stable configuration almost instantly.

## 4 | CONCLUSIONS

3D simulations of charged monodisperse particle suspensions subjected to a constant shear rate were carried out. To this end, our in-house code was extended by incorporating subgrid scale repulsive forces accounting for the EDLs about the charged particles and for the pH of the carrier liquid. The solids volume concentration, $\phi_v$, was varied between 6% and 52%, particle radii being 10 and 150 μm, with Reynolds number, $Re_p$, kept constant at the value 0.1. The electrolyte solution in which the particles were suspended had a pH of 9, 10, 11, and 12, respectively. Simulations were run for three values of the zeta potential, viz. $\psi_\delta = 0$ (i.e., no EDLs), $\psi_\delta = 30$ mV, and $\psi_\delta > 175$ mV.

Incorporating EDL forces, on top of the earlier subgrid scale LCs, slightly reduced the relative apparent suspension viscosity, although overall, up to some 30%–40% solids, the viscosities still largely follow the 1959 correlation of Krieger and Dougherty.[7] From about 40%

solids up to as high as 52%, however, the EDLs make the apparent viscosity level off and deviate from the Krieger and Dougherty correlation.

We demonstrated that this leveling off is related to a gradual transformation from, at dilute suspensions, a well-mixed homogeneous state comprising clusters of varying sizes into layers or chains of regular hexagonal structures at increasing solids fractions, most convincingly observed at $\phi_v = 52\%$. This elucidates that EDLs are rather successful in mitigating the role of agglomerates, clusters, and structures in increasing apparent suspension viscosity.

We found that pH (or ionic strength) of the carrier liquid and the EDLs about the particle as expressed by th Debye length to have opposite effffects on the repulsive interaction force between particles. We observed, at least at $\phi_v = 52\%$, a minimum in the apparent suspension viscosity at pH = 10 when the pertinent value of the nondimensional parameter $\kappa R_{\text{hyd}}$ was 355. Obviously, the pH of the liquid affects the thickness and the effectiveness of the EDLs.

We also performed a flow reversal study which showed that the suspension structures and the resulting apparent viscosity before and a sufficient time after the flow reversal are almost identical, or at least very similar. The EDLs did have a profound effect in the transition process right after the reversal: while after a flow reversal in the absence of EDLs the clusters have to be broken, reshuffled, and built

up again, with EDLs the particle chains remain separated and respond faster to a new state.

Several papers in the literature report differences between suspensions of monodisperse and bidisperse particles. Denn and Morris[28] report in their review paper that a bimodal particle size distribution leads to lower apparent suspension viscosities than a monodisperse suspension. They refer not only to experimental measurements[29] but also to computational simulations,[30] which indicate that such a lower viscosity is due to a reduced tendency toward clustering in comparison with monodisperse particles. Further work should be conducted to see whether bidispersity would affect the differences in structure between non-ionic and ionic suspensions that we have found.

## AUTHOR CONTRIBUTIONS

**Sudharsan Srinivasan:** Data curation (equal); investigation (lead); methodology (equal); software (lead); validation (equal); visualization (lead); writing—review and editing (equal). **Harry E. A. Van den Akker:** Conceptualization (equal); funding acquisition (lead); methodology (equal); project administration (lead); resources (equal); supervision (lead); validation (equal); writing—original draft (lead); writing—review and editing (equal). **Orest Shardt:** Conceptualization (equal); formal analysis (lead); investigation (equal); methodology (equal); resources (equal); software (supporting); supervision (equal); validation (equal); writing—review and editing (equal).

## ACKNOWLEDGMENTS

## DATA AVAILABILITY STATEMENT

Data available on request from the authors

## ORCID

*Sudharsan Srinivasan* https://orcid.org/0000-0002-7917-5852

*Harry E. A. Van den Akker* https://orcid.org/0000-0002-8143-5895

## REFERENCES

1. Chang SH, Ryan MH, Gupta RK. The effect of pH, ionic strength, and temperature on the rheology and stability of aqueous clay suspensions. *Rheola Acta*. 1993;32(3):263-269.
2. Tombácz E, Csanaky CS, Ill'es E. Polydisperse fractal aggregate formation in clay mineral and iron oxide suspensions, pH and ionic strength dependence. *Colloid Polym Sci*. 2001;279(5):484-492.
3. Gamal H, Elkatatny S, Basfar S, Al-Majed A. Effect of pH on rheological and filtration properties of water-based drilling fluid based on bentonite. *Sustainability*. 2019;11(23):6714.
4. Srinivasan S, Van den Akker HEA, Shardt O. Shear thickening and history-dependent rheology of monodisperse suspensions with finite inertia via an immersed boundary lattice Boltzmann method. *Int J Multiphase Flow*. 2020;125:103205.
5. Srinivasan S, Van den Akker HEA, Shardt O. Numerical simulations of dense granular suspensions in laminar flow under constant and varying shear rates. *Comput Fluids*. 2021;230:105115.
6. Aidun CK, Clausen JR. Lattice-Boltzmann method for complex flows. *Annu Rev Fluid Mech*. 2010;42:439-472.
7. Krieger IM, Dougherty TJ. A mechanism for non-Newtonian flow in suspensions of rigid spheres. *Trans Soc Rheol*. 1959;3:137-152.
8. Sierou A, Brady JF. Rheology and microstructure in concentrated non-colloidal suspensions. *J Rheol*. 2002;46(5):1031-1056.
9. Thorimbert Y, Marson F, Parmigiani A, Chopard B, Lätt J. Lattice Boltzmann simulation of dense rigid spherical particle suspensions using immersed boundary method. *Comput Fluids*. 2018;166:286-294.
10. Derjaguin BV, Landau L. Theory of the stability of strongly charged lyophobic sols and of the adhesion of strongly charged particles in solution of electrolytes. *Acta Physiochim USSR*. 1941;14:633.
11. Verwey EJW, Overbeek JTG. Theory of the stability of lyophobic colloids. *J Colloid Sci*. 1955;10(2):224-225.
12. Masliyah JH, Bhattacharjee S. *Electrokinetic and Colloid Transport Phenomena*. Wiley; 2006.
13. Berg JC. *An Introduction to Interfaces & Colloids: the Bridge to Nanoscience*. World Scientific Publishing Co.; 2010.
14. Srinivasan S, Van den Akker HEA, Shardt O. Inclusion of DLVO forces in simulations of non-Brownian solid suspensions: rheology and structure. *Int J Multiphase Flow*. 2022;149:103929.
15. Mari R, Seto R, Morris JF, Denn MM. Shear thickening, frictionless and frictional rheologies in non-Brownian suspensions. *J Rheol*. 2014;58:1693-1724.
16. Reasor DA, Clausen JR, Aidun CK. Rheological characterization of cellular blood in shear. *J Fluid Mech*. 2013;726:497-516.
17. Chen S, Doolen GD. Lattice Boltzmann method for fluid flows. *Annu Rev Fluid Mech*. 1998;30(1):329-364.
18. Ladd AJC. Numerical simulations of particulate suspensions via a discretized Boltzmann equation. Part 1. Theoretical foundation. *J Fluid Mech*. 1994;271:285-309.
19. Ladd AJC. Numerical simulations of particulate suspensions via a discretized Boltzmann equation. Part 2. Numerical results. *J Fluid Mech*. 1994;271:311-339.
20. Feng ZG, Michaelides EE. The immersed boundary-lattice Boltzmann method for solving fluid-particles interaction problems. *J Comput Phys*. 2004;195(2):602-628.
21. Krüger T, Kusumaatmaja H, Kuzmin A, Shardt O, Silva G, Viggen EM. *The Lattice Boltzmann Method: Principles and Practice*. Springer International Publishing; 2017.
22. Shan X, Chen H. Lattice Boltzmann model for simulating flows with multiple phases and components. *Phys Rev E*. 1993;47(3):1815-1819.
23. Srinivasan S. *Lattice Boltzmann Simulations of Dense Granular Suspensions*. PhD Thesis. School of Engineering, University of Limerick, Ireland. 2021.
24. Perkins E, Williams JR. Generalized spatial binning of bodies of different sizes. In: Cook BK, Jensen RP, eds. *Discrete Element Methods: Numerical Modeling of Discontinua*. American Society of Civil Engineers; 2002:52-55.
25. Williams JR, Perkins E, Cook B. A contact algorithm for partitioning N arbitrary sized objects. *Eng Comput*. 2004;21:235-248.
26. Liu Y, Naidu R, Ming H. Surface electrochemical properties of red mud (bauxite residue): zeta potential and surface charge density. *J Colloid Interface Sci*. 2013;394:451-457.
27. Gadala-Maria F, Acrivos A. Shear-induced structure in a concentrated suspension of solid spheres. *J Rheol*. 1980;24:799-814.

28. Denn MM, Morris JF. Rheology of non-Brownian suspensions. *Annu Rev Chem Biomol Eng*. 2014;5:203-228.

29. Chong JS, Christiansen EB, Baer AD. Rheology of concentrated suspensions. *J Appl Polym Sci*. 1971;15:2007-2021.

30. Chang C, Powell RL. Dynamic simulation of bimodal suspensions of hydro-dynamically interacting spherical particles. *J Fluid Mech*. 1993; 253:1-25.